

# A product shape manifold approach for optimizing piecewise-smooth shapes\*

Lidiya Pryymak<sup>1</sup>, Tim Suchan<sup>2</sup>, and Kathrin Welker<sup>3</sup>

<sup>1</sup>TU Bergakademie Freiberg, [lidiya.pryymak@math.tu-freiberg.de](mailto:lidiya.pryymak@math.tu-freiberg.de)

<sup>2</sup>Helmut Schmidt University, [suchan@hsu-hh.de](mailto:suchan@hsu-hh.de)

<sup>3</sup>TU Bergakademie Freiberg, [kathrin.welker@math.tu-freiberg.de](mailto:kathrin.welker@math.tu-freiberg.de)

## Abstract

Spaces where each element describes a shape, so-called shape spaces, are of particular interest in shape optimization and its applications. Theory and algorithms in shape optimization are often based on techniques from differential geometry. Challenges arise when an application demands a non-smooth shape, which is commonly-encountered as an optimal shape for fluid-mechanical problems. In order to avoid the restriction to infinitely-smooth shapes of a commonly-used shape space, we construct a space containing shapes in  $\mathbb{R}^2$  that can be identified with a Riemannian product manifold but at the same time admits piecewise-smooth curves as elements. We combine the new product manifold with an approach for optimizing multiple non-intersecting shapes. For the newly-defined shapes, adjustments are made in the known shape optimization definitions and algorithms to ensure their usability in applications. Numerical results regarding a fluid-mechanical problem constrained by the Navier-Stokes equations, where the viscous energy dissipation is minimized, show its applicability.

**Key words:** shape optimization, piecewise-smooth shape, Riemannian manifold, product manifold, Navier-Stokes equation

**AMS subject classifications:** 49Q10, 53C15, 58D10, 35Q30, 65K05

## 1 Introduction

Shape optimization is commonly-applied in engineering in order to optimize shapes w.r.t. to an objective functional that relies on the solution of a partial differential equation (PDE). The PDE is required to model the underlying physical phenomenon, e.g. elastic displacements due to loadings or fluid

---

\*This work has been partly supported by the German Research Foundation (DFG) within the priority program SPP 1962 under contract number WE 6629/1-1 and by the state of Hamburg (Germany) within the Landesforschungsförderung under project SEN-SUS with project number LFF-GK11.

movement due to pressure differences. Different methods are available for the shape optimization, however we focus on gradient-based techniques on shape spaces.

An ideal shape space would enable the usage of classical optimization methods like gradient descent algorithms. Since this is usually not the case, it is desirable to define a shape  $u$  to be an element of a Riemannian manifold. An important example of a smooth<sup>1</sup> manifold allowing a Riemannian structure is the shape space

$$B_e := B_e(S^1, \mathbb{R}^2) := \text{Emb}(S^1, \mathbb{R}^2)/\text{Diff}(S^1).$$

An element of  $B_e$  is a smooth simple closed curve in  $\mathbb{R}^2$ . The space was briefly investigated in [10]. The existence of Riemannian metrics, geodesics or, more generally, the differential geometric structure of  $B_e$  (cf., e.g. [11, 10]) reveals many possibilities like the computation of the shape gradient in shape optimization (cf., e.g. [15]). However, since an element of  $B_e$  is a smooth curve in  $\mathbb{R}^2$ , the shape space is in general not sufficient to carry out optimization algorithms on piecewise-smooth shapes, which are often encountered as an optimal shape for fluid-mechanical problems, see e.g. [14] for a prominent example. In particular, we are interested in shapes with kinks. Such piecewise-smooth shapes are generally not elements of a shape space that provides the desired geometrical properties for applications in shape optimization. Some effort has been put into constructing a shape space that contains non-smooth shapes, however so far only a diffeological space structure could be found, cf. e.g. [19, 20]. A further issue for many applications in shape optimization [1, 5, 8], such as the electrical impedance tomography, is to consider multi-shapes. A first approach for optimizing smooth multi-shapes has been presented in [6].

In this paper, we aim to construct a novel shape space holding a Riemannian structure for optimizing piecewise-smooth multi-shapes. The structure of the paper is as follows: In section 2, we extend the findings related to multi-shapes in [6] to a novel shape space considering piecewise-smooth shapes. Hereby, we use the fact that the space of simple, open curves

$$B_e([0, 1], \mathbb{R}^2) := \text{Emb}([0, 1], \mathbb{R}^2)/\text{Diff}([0, 1])$$

is a smooth manifold as well (cf. [9]) and interpret a closed curve with kinks as a glued-together curve of smooth, open curves, i.e., elements of  $B_e([0, 1], \mathbb{R}^2)$ . Moreover, we derive a shape optimization procedure on the novel shape space. In section 3, we apply the presented optimization technique to a shape optimization problem constrained by Navier-Stokes equations and present numerical results.

---

<sup>1</sup>Throughout this paper, the term smooth shall refer to infinite differentiability.

## 2 Product space for optimizing piecewise-smooth shapes

In this section, we aim to construct a gradient descent algorithm for optimizing piecewise-smooth multi-shapes, e.g. the multi-shape  $u = (u_1, u_2)$  from figure 1. In section 2.1, we therefore introduce a novel shape space which has the structure of a Riemannian product manifold. An optimization algorithm on the novel shape space is formulated in section 2.2.

### 2.1 Product shape space

In the following, we introduce a novel shape manifold, whose structure will later be used to optimize piecewise-smooth shapes. The construction of the novel shape space is based on a Riemannian product manifold. Therefore, we first investigate the structure of product manifolds.

We define  $(\mathcal{U}_i, G^i)$  to be Riemannian manifolds equipped with the Riemannian metrics  $G^i$  for all  $i = 1, \dots, N \in \mathbb{N}$ . The Riemannian metric  $G^i$  at the point  $p \in \mathcal{U}_i$  will be denoted by

$$G_p^i(\cdot, \cdot): T_p\mathcal{U}_i \times T_p\mathcal{U}_i \rightarrow \mathbb{R},$$

where  $T_p\mathcal{U}_i$  denotes the tangent space at a point  $p \in \mathcal{U}_i$ . We then define the product manifold as

$$\mathcal{U}^N := \mathcal{U}_1 \times \dots \times \mathcal{U}_N = \prod_{i=1}^N \mathcal{U}_i.$$

As shown in [6], for the tangent space of product manifolds it holds

$$T_{\tilde{u}}\mathcal{U}^N \cong T_{\tilde{u}_1}\mathcal{U}_1 \times \dots \times T_{\tilde{u}_N}\mathcal{U}_N.$$

Moreover, a product metric can be defined as

$$\mathcal{G}^N = \sum_{i=1}^N \pi_i^* G^i, \tag{1}$$

where  $\pi_i^*$  are the pushforwards associated with canonical projections. It is obvious to use the space  $B_e$  defined in section 1 to construct a specific product shape space. An issue arises for non-smooth shapes, e.g. the shape  $u_1$  from figure 1. To fix this issue, we now introduce the new multi-shape space for  $s$  shapes built on the Riemannian product manifold  $\mathcal{U}^N$ .

**Definition 2.1.** Let  $(\mathcal{U}_i, G^i)$  be Riemannian manifolds equipped with Riemannian metrics  $G^i$  for all  $i = 1, \dots, N$ . Moreover,  $\mathcal{U}^N := \prod_{i=1}^N \mathcal{U}_i$ . For

$s \in \mathbb{N}$ , we define the  $s$ -dimensional shape space on  $\mathcal{U}^N$  by

$$M_s(\mathcal{U}^N) := \{u = (u_1, \dots, u_s) \mid u_j \in \prod_{l=k_j}^{k_j+n_j-1} \mathcal{U}_l, \sum_{j=1}^s n_j = N \text{ and} \\ k_1 = 1, k_{j+1} = k_j + n_j \forall j = 1, \dots, s-1\}.$$

With definition 2.1, an element in  $M_s(\mathcal{U}^N)$  is defined as a group of  $s$  shapes  $u_1, \dots, u_s$ , where each shape  $u_j$  is an element of the product of  $n_j$  smooth manifolds. For  $\mathcal{U}_l = B_\epsilon([0, 1], \mathbb{R}^2)$  for  $l = 1, \dots, 12$  and  $\mathcal{U}_{13} = B_\epsilon(S^1, \mathbb{R}^2)$ , we can define the shapes presented in figure 1 by  $(u_1, u_2) \in M_2(\mathcal{U}^{13})$ , where  $u_1 \in \prod_{l=1}^{12} \mathcal{U}_l$  and  $u_2 \in \mathcal{U}_{13}$ .

For applications of definition 2.1 in shape optimization problems, it is of great interest to look at the tangent space of  $M_s(\mathcal{U}^N)$ . Since any element  $u = (u_1, \dots, u_s) \in M_s(\mathcal{U}^N)$  can be understood as an element  $\tilde{u} = (\tilde{u}_1, \dots, \tilde{u}_N) \in \mathcal{U}^N$ , we set  $T_u M_s(\mathcal{U}^N) = T_{\tilde{u}} \mathcal{U}^N$  and

$$G_u(\varphi, \psi) = G_{\tilde{u}}(\varphi, \psi) \quad \forall \varphi, \psi \in T_u M_s(\mathcal{U}^N) = T_{\tilde{u}} \mathcal{U}^N.$$

Next, we consider shape optimization problems, i.e., we investigate so-called shape functionals. A shape functional on  $M_s(\mathcal{U}^N)$  is given by  $j: M_s(\mathcal{U}^N) \rightarrow \mathbb{R}$ ,  $u \mapsto j(u)$ . In the following paragraph, we investigate solution techniques for shape optimization problems, i.e., for problems of the form

$$\min_{u \in M_s(\mathcal{U}^N)} j(u). \quad (2)$$

## 2.2 Optimization technique on $M_s(\mathcal{U}^N)$ for optimizing piecewise-smooth shapes

A theoretical framework for shape optimization depending on multi-shapes is presented in [6], where the optimization variable can be represented as a multi-shape belonging to a product shape space. Among other things, a multi-pushforward and multi-shape gradient are defined; however, each shape is assumed to be an element of one shape space. In contrast, definition 2.1 also allows that a shape itself is represented by a product shape space. Therefore, we need to adapt the findings in [6] to our setting.

To derive a gradient descent algorithm for a shape optimization problem as in (2), we need a definition for differentiating a shape functional mapping from a smooth manifold to  $\mathbb{R}$ . For smooth manifolds, this is achieved using a pushforward.

**Definition 2.2.** For each shape  $u \in M_s(\mathcal{U}^N)$ , the multi-pushforward of a shape functional  $j: M_s(\mathcal{U}^N) \rightarrow \mathbb{R}$  is given by the map

$$(j_*)_u: T_u M_s(\mathcal{U}^N) \rightarrow \mathbb{R}, \quad \varphi \mapsto \frac{d}{dt} j(\varphi(t))_{t=0} = (j \circ \varphi)'(0).$$

Thanks to the multi-pushforward, we can define the so-called multi-shape gradient, which is required for optimization algorithms.

**Definition 2.3.** The multi-shape gradient for a shape functional  $j: M_s(\mathcal{U}^N) \rightarrow \mathbb{R}$  at the point  $u \in M_s(\mathcal{U}^N)$  is given by  $\psi \in T_u M_s(\mathcal{U}^N)$  satisfying

$$\mathcal{G}_u^N(\psi, \varphi) = (j_*)_u \varphi \quad \forall \varphi \in T_{\tilde{u}} M_s(\mathcal{U}^N).$$

We are now able to formulate a gradient descent algorithm on  $M_s(\mathcal{U}^N)$  similar to the one presented in [6]. For updating the multi-shape  $u$  in each iteration, the multi-exponential map

$$\exp_u^N: T_u M_s(\mathcal{U}^N) \rightarrow M_s(\mathcal{U}^N), \quad \varphi = (\varphi_1, \dots, \varphi_N) \mapsto (\exp_{\tilde{u}_1} \varphi_1, \dots, \exp_{\tilde{u}_N} \varphi_N)$$

is used. The algorithm is depicted in algorithm 1.

---

**Algorithm 1** Gradient descent algorithm on  $M_s(\mathcal{U}^N)$  with Armijo backtracking line search to solve (2)

---

**Input:** Initial shape  $u = (u_1, \dots, u_s) = (\tilde{u}_1, \dots, \tilde{u}_N) = \tilde{u}$ , constants for Armijo backtracking and  $\epsilon > 0$  for break condition

- 1: **while**  $\|v\|_{\mathcal{G}^N} > \epsilon$  **do**
  - 2:     Compute the multi-shape gradient  $v$  with respect to  $\mathcal{G}^N$
  - 3:     Compute stepsize  $\alpha$  with Armijo backtracking
  - 4:      $u \leftarrow \exp_u^N(-\alpha v)$
  - 5: **end while**
- 

So far, we have derived an optimization algorithm on  $M_s(\mathcal{U}^N)$ , i.e., an algorithm for optimizing a non-intersecting group of shapes, where each shape is an element of a product manifold with a varying number of factor spaces. With the main goal of this section in mind, we need to further restrict the choice of shapes in  $M_s(\mathcal{U}^N)$  to glued-together piecewise-smooth shapes: We assume that  $\mathcal{U}_i$  is either  $B_e(S^1, \mathbb{R}^2)$  or  $B_e([0, 1], \mathbb{R}^2)$ . Moreover, we assume that each shape  $(u_1, \dots, u_s)$  is closed, where  $u = (u_1, \dots, u_s)$  is chosen from  $M_s(\mathcal{U}^N)$ . By that we mean that if a shape is  $u_j \in \prod_{l=k_j}^{k_j+n_j-1} \mathcal{U}_l$ ,

then either

$$n_j = 1 \text{ and } \mathcal{U}_{k_j} = B_e(S^1, \mathbb{R}^2)$$

or

$$\mathcal{U}_l = B_e([0, 1], \mathbb{R}^2) \quad \forall l = k_j, \dots, k_j + n_j - 1 \text{ and for}$$

$$u_j = (u_{k_j}, \dots, u_{k_j+n_j-1}), \text{ it holds that}$$

$$u_{k_j+h}(1) = u_{k_j+h+1}(0) \quad \forall h = 0, \dots, n_j - 2 \text{ and } u_{k_j}(0) = u_{k_j+n_j-1}(1).$$

Finally, we want to address another important issue in shape optimization algorithms: the development of kinks in smooth shapes over the course

of the optimization. If we view a smooth initial shape, e.g.  $u_2$  from figure 1, as an element in  $B_e(S^1, \mathbb{R}^2)$  no kinks can arise during the optimization of the shape. An approach to fix this issue for applications, where the developments of kinks in shapes is desired, is to approximate a smooth shape with elements of  $B_e([0, 1], \mathbb{R}^2)$ . A simple but sufficient choice is using initially straight lines connecting locations of possible kinks. In this manner, the multi-shape  $u = (u_1, u_2)$  from figure 1 would be an element of

$$M_2(\mathcal{U}^{12+l_1+l_2}), \text{ where } l_1, l_2 \in \mathbb{N} \text{ and} \\ u_1 \in \prod_{l=1}^{12+l_1} \mathcal{U}_l = B_e([0, 1], \mathbb{R}^2)^{12+l_1}, u_2 \in \prod_{l=13+l_1}^{12+l_1+l_2} \mathcal{U}_l = B_e([0, 1], \mathbb{R}^2)^{l_2}. \quad (3)$$

### 3 Application to Navier-Stokes flow

In the following, we apply algorithm 1 to a shape optimization problem constrained by steady-state Navier-Stokes equations and geometrical constraints. In section 3.1, we briefly describe the numerical implementation of algorithm 1. Afterwards, we formulate the optimization problem that will be considered for the numerical studies in section 3.2, and finally, in section 3.3, we describe the numerical results.

#### 3.1 Adjustments of algorithm 1 for numerical computations

In order to ensure the numerical applicability of algorithm 1, adjustments must be made. We define the space  $\mathcal{W} := \{\mathbf{W} \in H^1(D_{\mathbf{u}}, \mathbb{R}^2) \mid \mathbf{W} = \mathbf{0} \text{ on } \partial D_{\mathbf{u}} \setminus \mathbf{u}\}$ , and similarly to [6], we use an optimization approach based on partial shape derivatives, together with the Steklov-Poincaré metric in equation (1). The Steklov-Poincaré metric is defined in [16] and yields  $\mathcal{G}^i(\mathbf{V}|_u, \mathbf{W}|_u) = a(\mathbf{V}, \mathbf{W})$  with a symmetric and coercive bilinear form  $a: \mathcal{W} \times \mathcal{W}$ . We replace the multi-shape gradient with the mesh deformation  $\mathbf{V} \in \mathcal{W}$ , which is obtained by replacing the multi-pushforward with the multi-shape derivative<sup>2</sup> in definition 2.3. A common choice for the bilinear form when using the Steklov-Poincaré metric is linear elasticity

$$\int_{D_{\mathbf{u}}} \varepsilon(\mathbf{V}) : \mathbf{C} : \varepsilon(\mathbf{W}) \, d\mathbf{x} = dj(\mathbf{u})[\mathbf{W}] \quad \forall \mathbf{W} \in \mathcal{W}, \quad (4)$$

where  $\varepsilon(\mathbf{V}) = \text{sym grad}(\mathbf{V})$  and  $\mathbf{C}$  describes the linear elasticity tensor,  $\mathbf{A} : \mathbf{B}$  is the standard Frobenius inner product and  $dj(\mathbf{u})[\mathbf{W}]$  denotes the shape derivative of  $j$  at  $\mathbf{u}$  in direction  $\mathbf{W}$ . Due to the equivalence of the Steklov-Poincaré metric and the bilinear form  $a$ , we replace the  $\mathcal{G}^N$ -norm in the stopping criterion of the algorithm 1 with the  $H^1$ -norm in  $D_{\mathbf{u}}$ . Finally, since the exponential map used in algorithm 1 is an expensive operation, it

<sup>2</sup>We refer to [6] for the definition and details about the multi-shape derivative.

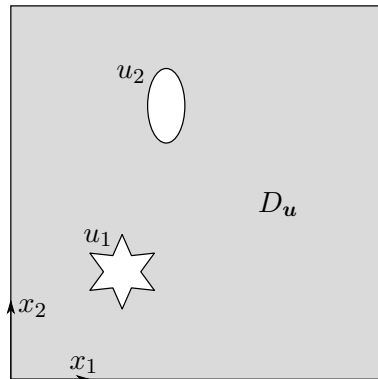


Figure 1: Sketch of two shapes  $u_1$ ,  $u_2$  surrounded by a domain  $D_{\mathbf{u}} \subset \mathbb{R}^2$ .

is common to replace it by a so-called retraction. In our computations, we use the retraction introduced in [17].

### 3.2 Model formulation

We consider the problem

$$\min_{\mathbf{u} \in M_s(\mathcal{U}^N)} j(\mathbf{u}) := \min_{\mathbf{u} \in M_s(\mathcal{U}^N)} \int_{D_{\mathbf{u}}} \frac{\mu}{2} \nabla \mathbf{v} : \nabla \mathbf{v} \, d\mathbf{x}, \quad (5)$$

where we constrain the optimization problem by the Navier-Stokes equations and choose  $M_s(\mathcal{U}^N)$  as in (3). The state is denoted as  $\mathbf{y} = (\mathbf{v}, p)$  for which the Navier-Stokes equations can be found in standard literature and will be omitted here for brevity. The material constants dynamic viscosity and density are defined as  $\mu = 1.81$  and  $\rho = 1.2 \cdot 10^5$ , respectively. We choose homogenous Dirichlet boundary conditions on the top and bottom boundary as well as on both shapes. The right boundary is modelled as homogenous Neumann, and the left boundary has the inhomogenous Dirichlet boundary condition  $\mathbf{v} = (0.08421 x_2 (x_2 - 1), 0)^\top$ . We choose the hold-all domain  $D = (0, 1)^2$ , in which two shapes  $u_1$  and  $u_2$  are embedded as shown in figure 1 with barycenters at  $(0.3, 0.3)^\top$  and  $(0.45, 0.75)^\top$ , respectively.

Additional geometrical constraints are required in order to avoid trivial solutions, see e.g. [12, 13], which are implemented as inequality constraints with an Augmented Lagrange approach as described in [18]. We restrict the area of each shape  $\text{vol}(u_i)$  to be at 100% initial area. Further, the barycenter  $\text{bary}(u_1)$  is constrained to stay between  $(-0.03, -0.05)^\top$  and  $(0.04, 0.03)^\top$  of the initial position in  $x$  and  $y$  direction, respectively, and the barycenter  $\text{bary}(u_2)$  to stay between  $(-0.075, -0.02)^\top$  and  $(0.02, 0.05)^\top$  of the initial position.

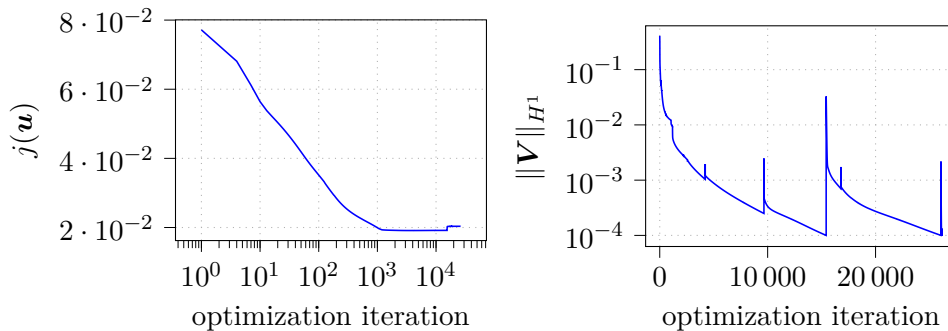


Figure 2: Optimization results: objective functional (left) and  $H^1$ -norm of the mesh deformation (right).

### 3.3 Numerical results

The computational domain is discretized with 3512 nodes and 7026 triangular elements using Gmsh [7] with standard Taylor-Hood elements. An automatic remesher is available in case the mesh quality deteriorates below a threshold. The optimization is performed in FEniCS 2019.1.0 [2]. We use a Newton solver and solve the linearized system of equations using MUMPS 5.5.1 [3, 4]. Armijo backtracking is performed as described in algorithm 1 with  $\tilde{\alpha} = 0.0125$ ,  $\sigma = 10^{-4}$  and  $\tilde{\rho} = \frac{1}{10}$ . The stopping criterion for each gradient descent is reached when the  $H^1$ -norm of the mesh deformation is at or below  $10^{-4}$ . The objective functional and the  $H^1$ -norm of the mesh deformation over the course of the optimization are shown in figure 2 and the magnitude of the fluid velocity in the computational domain before, during, and after optimization can be found in figure 3. The optimized shapes can be seen in figure 3 on the right. Over the course of the optimization we observe a reduction of the objective functional by approximately 74%. The norm of the mesh deformation shows an exponential decrease, similar to a classical gradient descent algorithm. The peaks are caused by remeshing or by the adjustment of Augmented Lagrange parameters. Initially, the optimizer is mainly concerned with obtaining an approximate optimized shape, see figure 3b–3d, while the exact fulfillment of geometrical constraints is less relevant. The later stages optimize small features like the leading and trailing edge of the shape, see figure 3e, any suboptimal kinks that were still remaining are removed, and in figure 3f the geometrical constraints are fulfilled with an infeasibility of below  $10^{-6}$  after  $k = 7$  Augmented Lagrange iterations.



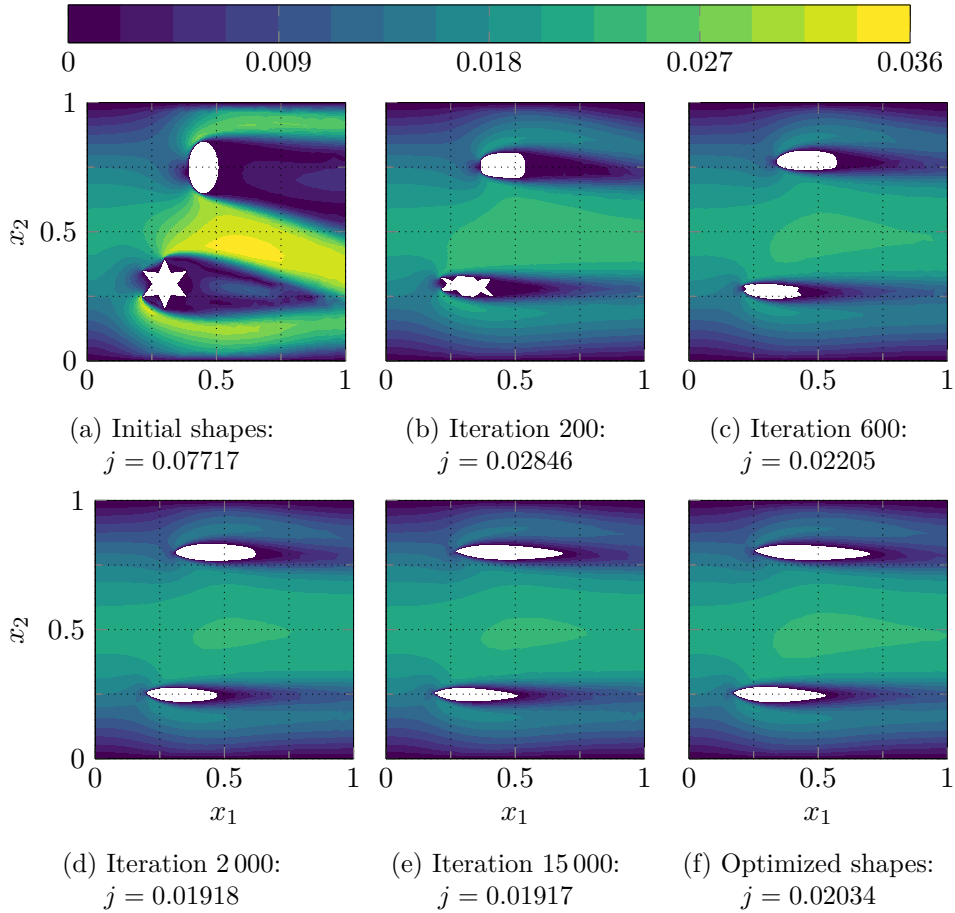


Figure 3: Fluid velocity magnitude at different stages of the optimization. Figure 3f has an increased objective functional value in comparison to figure 3d and 3e, however it fulfills the geometrical constraints while the others do not yet.

## 4 Conclusion

A novel shape space  $M_s(\mathcal{U}^N)$  that provides both, a Riemannian structure and a possibility to consider glued-together shapes (in particular, shapes with kinks) is introduced. Additionally, an optimization algorithm, based on findings from [6], is formulated. The new algorithm is applied to solve an optimization problem constrained by the Navier-Stokes equations with additional geometrical inequality constraints, where we have observed a strong reduction of the objective functional and convergence of the gradient descent on  $M_s(\mathcal{U}^N)$  similar to a classical gradient descent algorithm. Forthcoming research should involve an investigation of the development of the shapes' overlaps (glued-together points) over the course of the optimization. Moreover, convergence statements need to be investigated.

## References

- [1] Y.F. Albuquerque, A. Laurain, and K. Sturm. A shape optimization approach for electrical impedance tomography with point measurements. *Inverse Probl*, 36(9):095006, 2020. doi:10.1088/1361-6420/ab9f87.
- [2] M. Alnæs, J. Blechta, J. Hake, A. Johansson, B. Kehlet, A. Logg, C. Richardson, J. Ring, M.E. Rognes, and G.N. Wells. The FEniCS Project Version 1.5. *Archive of Numerical Software*, 3(100), 2015. doi:10.11588/ans.2015.100.20553.
- [3] P.R. Amestoy, I.S. Duff, J. Koster, and J.-Y. L'Excellent. A fully asynchronous multifrontal solver using distributed dynamic scheduling. *SIAM J Matrix Anal Appl*, 23(1):15–41, 2001. doi:10.1137/S0895479899358194.
- [4] P.R. Amestoy, A. Guermouche, J.-Y. L'Excellent, and S. Pralet. Hybrid scheduling for the parallel solution of linear systems. *Parallel Comput*, 32(2):136–156, 2006. doi:10.1016/j.parco.2005.07.004.
- [5] M. Cheney, D. Isaacson, and J.C. Newell. Electrical impedance tomography. *SIAM Rev Soc Ind Appl Math*, 41(1):85–101, 1999. doi:10.1137/S0036144598333613.
- [6] C. Geiersbach, E. Loayza-Romero, and K. Welker. PDE-constrained shape optimization: Towards product shape spaces and stochastic models. In K. Chen, C.-B. Schönlieb, X.-C. Tai, and L. Younes, editors, *Handbook of Mathematical Models and Algorithms in Computer Vision and Imaging*, pages 1–46. Springer International Publishing, 2022. doi:10.1007/978-3-030-03009-4\_120-1.
- [7] C. Geuzaine and J.-F. Remacle. Gmsh: A 3-D finite element mesh generator with built-in pre- and post-processing facilities. *Int J Numer Methods Eng*, 79(11):1309–1331, 2009. doi:10.1002/nme.2579.
- [8] O. Kwon, E.J. Woo, J.-R. Yoon, and J.K. Seo. Magnetic resonance electrical impedance tomography (mreit): simulation study of j-substitution algorithm. *IEEE Trans Biomed Eng*, 49(2):160–167, 2002. doi:10.1109/10.979355.
- [9] P.W. Michor. *Manifolds of differentiable mappings*, volume 3. Shiva mathematics series, 1980. URL: [https://www.mat.univie.ac.at/~michor/manifolds\\_of\\_differentiable\\_mappings.pdf](https://www.mat.univie.ac.at/~michor/manifolds_of_differentiable_mappings.pdf).
- [10] P.W. Michor and D.B. Mumford. Riemannian geometries on spaces of plane curves. *J. Eur. Math. Soc.*, 8:1–48, 2006. doi:10.4171/JEMS/37.

- [11] P.W. Michor and D.B. Mumford. An overview of the Riemannian metrics on spaces of curves using the Hamiltonian approach. *Appl Comput Harmon Anal*, 23(1):74–113, 2007. doi:10.1016/j.acha.2006.07.004.
- [12] B. Mohammadi and O. Pironneau. *Applied Shape Optimization for Fluids*. Oxford University Press, 2009. doi:10.1093/acprof:oso/9780199546909.001.0001.
- [13] P.M. Müller, N. Kühl, M. Siebenborn, K. Deckelnick, M. Hinze, and T. Rung. A novel  $p$ -harmonic descent approach applied to fluid dynamic shape optimization. *Struct Multidiscipl Optim*, 64(6):3489–3503, 2021. doi:10.1007/s00158-021-03030-x.
- [14] O. Pironneau. On optimum profiles in Stokes flow. *J Fluid Mech*, 59(1):117–128, 1973. doi:10.1017/s002211207300145x.
- [15] V.H. Schulz. A Riemannian view on shape optimization. *Found Comput Math*, 14(3):483–501, 2014. doi:10.1007/s10208-014-9200-5.
- [16] V.H. Schulz, M. Siebenborn, and K. Welker. Efficient PDE constrained shape optimization based on Steklov-Poincaré-type metrics. *SIAM J Optim*, 26(4):2800–2819, 2016. doi:10.1137/15m1029369.
- [17] V.H. Schulz and K. Welker. On optimization transfer operators in shape spaces. In V. Schulz and D. Seck, editors, *Shape Optimization, Homogenization and Optimal Control*, pages 259–275. Springer International Publishing, 2018. doi:10.1007/978-3-319-90469-6\_13.
- [18] D. Steck. *Lagrange multiplier methods for constrained optimization and variational problems in Banach spaces*. PhD thesis, Universität Würzburg, 2018. URL: <https://opus.bibliothek.uni-wuerzburg.de/frontdoor/index/index/year/2018/docId/17444>.
- [19] K. Welker. *Efficient PDE constrained shape optimization in shape spaces*. PhD thesis, Universität Trier, 2016. doi:10.25353/ubtr-xxxx-6575-788c/.
- [20] K. Welker. Suitable spaces for shape optimization. *Appl Math Optim*, 84(S1):869–902, 2021. doi:10.1007/s00245-021-09788-2.